**ORIGINAL ARTICLE**

# ST6GAL1–mediated aberrant sialylation promotes prostate cancer progression

Emma Scott[1], Emily Archer Goode[1], Rebecca Garnham[1], Kirsty Hodgson[1], Margarita Orozco-Moreno[1],
Helen Turner[2], Karen Livermore[1], Kyla Putri Nangkana[1], Fiona M Frame[3], Abel Bermudez[4],
Fernando Jose Garcia Marques[4], Urszula L McClurg[5], Laura Wilson[6], Huw Thomas[6], Adriana Buskin[6],
Anastasia Hepburn[6], Adam Duxfield[1], Kayla Bastian[1], Hayley Pye[7], Hector M Arredondo[8], Gerald Hysenaj[1],
Susan Heavey[7], Urszula Stopka-Farooqui[7], Aiman Haider[9], Alex Freeman[9], Saurabh Singh[10], Edward W Johnston[10],
Shonit Punwani[10], Bridget Knight[11], Paul McCullagh[12], John McGrath[13], Malcolm Crundwell[13], Lorna Harries[14],
Rakesh Heer[6,15], Norman J Maitland[3], Hayley Whitaker[7], Sharon Pitteri[4], Dean A Troyer[16], Ning Wang[8],
David J Elliott[1], Richard R Drake[17] and Jennifer Munkley[1]*

1  Newcastle University Centre for Cancer, Newcastle University Institute of Biosciences, Newcastle, UK
2  Cellular Pathology, The Royal Victoria Infirmary, Newcastle upon Tyne, UK
3  Cancer Research Unit, Department of Biology, University of York, North Yorkshire, UK
4  Canary Center at Stanford for Cancer Early Detection, Department of Radiology, Stanford University, Palo Alto, CA, USA
5  Institute of Systems, Molecular & Integrative Biology, University of Liverpool, Liverpool, UK
6  Newcastle University Centre for Cancer, Translational and Clinical Research Institute, Paul O'Gorman Building, Newcastle University, Newcastle upon Tyne, UK
7  Molecular Diagnostics and Therapeutics Group, Charles Bell House, Division of Surgery and Interventional Science, University College London, London, UK
8  The Mellanby Centre for Musculoskeletal Research, Department of Oncology and Metabolism, The University of Sheffield, Sheffield, UK
9  Department of Pathology, UCLH NHS Foundation Trust, London, UK
10  UCL Centre for Medical Imaging, Charles Bell House, University College London, London, UK
11  NIHR Exeter Clinical Research Facility, Royal Devon and Exeter NHS Foundation Trust, Exeter, UK
12  Department of Pathology, Royal Devon and Exeter NHS Foundation Trust, Exeter, UK
13  Exeter Surgical Health Services Research Unit, Royal Devon and Exeter NHS Foundation Trust, Exeter, UK
14  Institute of Biomedical and Clinical Sciences, Medical School, College of Medicine and Health, University of Exeter, Exeter, UK
15  Department of Urology, Freeman Hospital, The Newcastle upon Tyne Hospitals NHS Foundation Trust, Newcastle upon Tyne, UK
16  Cancer Biology and Infectious Disease Research Center, Eastern Virginia Medical School, Norfolk, VA, USA
17  Department of Cell and Molecular Pharmacology, Medical University of South Carolina, Charleston, SC, USA

*Correspondence to: J Munkley, Newcastle University Centre for Cancer, Newcastle University Institute of Biosciences, Newcastle, NE1 3BZ, UK.
E-mail: jennifer.munkley@ncl.ac.uk

## Abstract

Aberrant glycosylation is a universal feature of cancer cells, and cancer–associated glycans have been detected in virtually every cancer type. A common change in tumour cell glycosylation is an increase in $\alpha2,6$ sialylation of *N*–glycans, a modification driven by the sialyltransferase ST6GAL1. ST6GAL1 is overexpressed in numerous cancer types, and sialylated glycans are fundamental for tumour growth, metastasis, immune evasion, and drug resistance, but the role of ST6GAL1 in prostate cancer is poorly understood. Here, we analyse matched cancer and normal tissue samples from 200 patients and verify that ST6GAL1 is upregulated in prostate cancer tissue. Using MALDI imaging mass spectrometry (MALDI–IMS), we identify larger branched $\alpha2,6$ sialylated *N*–glycans that show specificity to prostate tumour tissue. We also monitored ST6GAL1 in plasma samples from >400 patients and reveal ST6GAL1 levels are significantly increased in the blood of men with prostate cancer. Using both *in vitro* and *in vivo* studies, we demonstrate that ST6GAL1 promotes prostate tumour growth and invasion. Our findings show ST6GAL1 introduces $\alpha2,6$ sialylated *N*–glycans on prostate cancer cells and raise the possibility that prostate cancer cells can secrete active ST6GAL1 enzyme capable of remodelling glycans on the surface of other cells. Furthermore, we find $\alpha2,6$ sialylated *N*–glycans expressed by prostate cancer cells can be targeted using the sialyltransferase inhibitor P–3F$_{AX}$–Neu5Ac. Our study identifies an important role for ST6GAL1 and $\alpha2,6$ sialylated *N*–glycans in prostate cancer progression and highlights the opportunity to inhibit abnormal sialylation for the development of new prostate cancer therapeutics.

© 2023 The Authors. *The Journal of Pathology* published by John Wiley & Sons Ltd on behalf of The Pathological Society of Great Britain and Ireland.

Keywords: ST6GAL1; prostate cancer; glycosylation; sialylation; sialic acid; *N*–glycans

## Introduction

Prostate cancer is the most common cancer in males and claims the lives of more than 350,000 men every year [1]. The androgen receptor (AR) plays an essential role in the normal growth and development of the prostate gland, as well as in carcinogenesis [2]. First-line treatment for advanced prostate cancer is androgen deprivation therapy (ADT), but unfortunately most tumours progress to an aggressive state, known as castration-resistant prostate cancer (CRPC). Numerous second-generation ADT treatments, such as abiraterone [3,4], enzalutamide [5,6], and, more recently, darolutamide [7], are available for CRPC; however, nearly all patients will also develop resistance to these treatments [8]. New therapies for advanced prostate cancer are urgently needed and could improve patient quality of life and survival times.

Glycosylation is the most common post-translational modification of both membrane bound and secreted proteins [9]. Glycans play key roles in many biological processes and are fundamental regulators of signalling pathways, cell differentiation, immune recognition and host-pathogenic interactions [10–12]. Aberrant glycosylation is a hallmark of cancer and not just a consequence but also a driver of the malignant phenotype, directly impacting key processes supporting tumour progression, metastasis, and immune evasion [13]. Glycans hold huge translational potential and are already the focus of several clinical trials [14].

A common change in tumour cell glycosylation is an increase in α2,6 sialylation on *N*-glycans, a modification driven by the sialyltransferase enzyme ST6GAL1 [15–17]. ST6GAL1 plays a critical role in many cancers, where it is linked to aggressive disease and poor patient prognosis [18–20]. However, the role of ST6GAL1 in prostate cancer is poorly understood. Here, we verify that ST6GAL1 is upregulated in prostate cancer and further show that larger branched α2,6 sialylated *N*-glycans show specificity to prostate tumour tissue. We also find ST6GAL1 is upregulated in the blood of men with prostate cancer. Using both *in vitro* and *in vivo* studies, we find ST6GAL1 can promote prostate cancer cell invasion and tumour growth. Furthermore, we show ST6GAL1 regulates α2,6-linked sialylation of *N*-glycans in prostate cancer cells and reveal the potential for an extracellular function for ST6GAL1 in prostate cancer. Finally, we demonstrate that the action of ST6GAL1 can be targeted using the sialyltransferase inhibitor P-3FaX-Neu5Ac. Our findings identify an important role for ST6GAL1 and α2,6 sialylated *N*-glycans in prostate cancer progression and highlight the opportunity to exploit aberrant sialylation to develop new treatment strategies for men with prostate cancer.

## Materials & methods

### Immunohistochemistry

ST6GAL1 levels were monitored in a previously published tissue microarray (TMA) [21] consisting of prostatectomy tissue from 200 cases of prostate cancer and matched normal tissue (four cores each). Antigen retrieval was performed by pressure cooking for 90 s in 10 mM citrate pH 6.0 (Sigma-Aldrich, Gillingham, Dorset, UK, C9999) followed by staining with ST6GAL1 antibody (Abgent, San Diego, CA, USA, AP19891c, 1:6000). Nuclei were counterstained with haematoxylin (Sigma-Aldrich, 51275). The TMA was scored using the 0–300 Histoscore score method [22,23]. Only epithelial cells were scored. ST6GAL1 antibody was validated using peptide blocking with recombinant protein and formalin-fixed paraffin-embedded (FFPE) cell pellets with knockdown of ST6GAL1 (supplementary material, Figure S2).

### Prostate tissues used for MALDI imaging mass spectrometry (IMS)

A prostate cancer TMA was constructed using the guidelines reported by the Canary Foundation [24] and the Eastern Virginia Medical School site. Three 1-mm tumour cores from 42 FFPE prostate tumour tissues were selected for inclusion. All samples were collected from patients after informed consent was obtained following Institutional Review Board-approved protocols at Urology of Virginia and the Eastern Virginia Medical School. Personal information or identifiers beyond diagnosis and lab results were not available to the laboratory investigators. Two de-identified FFPE prostate tumour tissues of Gleason grade 7 (3 + 4) were obtained from the Hollings Cancer Center Tissue and Analysis Biorepository at the Medical University of South Carolina.

### *N*-glycan MALDI-IMS and sialic acid stabilisation

Following deparaffinisation, the FFPE prostate tissue and TMA slides were incubated with 0.2 ml 0.25 M *N*-(3-dimethylaminopropyl)-*N*'-ethylcarbodiimide (Sigma-Aldrich, 39391), 0.5 M 1-hydroxybenzotriazole hydrate (Sigma-Aldrich), and 0.25 M dimethylamine (Sigma-Aldrich) in dimethyl sulfoxide (Sigma-Aldrich) at 60 °C for 1 h, as previously described [25]. This results in amidation of α2,6 sialylated *N*-glycans and a + 27 mass unit shift. After rinsing and a second amidation reaction with ammonium hydroxide for stabilising α2,3 sialylated *N*-glycans [25], the tissues were prepared for antigen retrieval and spraying with a molecular coating of PNGase F using a standardised and previously published protocol [26,27]. After digestion for 2 h at 37 °C, 7 mg/ml

α-cyano-4-hydroxycinnamic acid matrix in 50% acetonitrile/0.1% trifluoroacetic acid was applied to the deglycosylated slides. A trapped ion-mobility time of flight fleX trapped ion mobility separated quadrupole time of flight mass spectrometer (Bruker Daltonics, Bremen, Germany) equipped with a 10-kHz SmartBeam 3D laser (Bruker Daltonics) operating in positive mode with a spot size of 20 μm was used to detect released *N*-glycans at a high-resolution 40 μm raster. After acquisition, spectra were imported to SCiLS Lab 2022b Pro (Bruker Daltonics) for processing and visualisation of mass spectrometry (MS) imaging data normalised to total ion count. Spectra were annotated by matching peaks against an in-house N-glycan database [28] that included amidated sialic acid isomers. Quantification was performed by total ion count normalisation of the data; then the glycan intensities of each tissue core were extracted using Bruker SCiLS software (version 2022b).

### Detection of ST6GAL1 in serum and plasma

Human ST6GAL1 sandwich ELISA kits were purchased from Cambridge Bioscience (RayBioTech, USA, ELH-ST6GAL1-1). Samples and standards were assayed in duplicate according to the manufacturer's protocol. Cohort 1: EDTA blood samples were collected with ethics approval through the NIHR Exeter Clinical Research Facility tissue bank (Ref: STB20) during standard routine National Health Service (NHS) clinical practice and spun (at least 30 min after collection) at $4,500 \times g$ for 10 min. The separated plasma was removed, aliquoted, and stored at $-80\,°C$. Written informed consent for the use of biological samples was provided by all patients. Cohort 2: Patient plasma samples were collected with ethical permission from Castle Hill Hospital (Cottingham, Hull) (ethics number: 07/H1304/121) and prepared using Histopaque (Sigma-Aldrich, 1077) as per the manufacturer's instructions (samples were spun at $600 \times g$ for 15 min at room temperature). Use of patient tissue was approved by the local research ethics committees. Patients gave informed consent, and all patient samples were anonymised. Cohort 3: The INNOVATE trial (combIning advaNces in imagiNg with biOmarkers for improVed diagnosis of Aggressive prosTate cancer) (ClinicalTrials.gov: NCT02689271) is a prospective cohort study evaluating the use of fluid biomarkers and mpMRI to the diagnostic pathway for suspected prostate cancer [29,30]. The blood samples used in this study were collected in plasma preparation tubes with K₂EDTA gel additive and BD Hemogard closure ($16 \times 100$ mm volume 8.5 ml vacutainer) (Fisher, Loughborough, UK, 12977696). Samples were separated for 20 min at 3,300 rpm ($2,118 \times g$) at $4\,°C$. 1-ml aliquots were frozen at $-80\,°C$. The average time between collection from the patient and being frozen was 1 h and 42 min (minimum 55 min, maximum 4 h).

### Cell culture and creation of stable cell lines

Cell culture and the cell lines used were as described previously [31]. Stable cell lines were created using lentiviral transduction. For ST6GAL1 knockdown, shRNA lentiviral particles were purchased from Santa Cruz (Heidelberg, Germany) (ST6GAL1 shRNA sc-42804 and Control shRNA sc-108080). Transductions were carried out according to the manufacturer's instructions using MOI = 5. For ST6GAL1 overexpression, Lentifect purified lentiviral particles were purchased from Tebu-Bio (Le Perray-en-Yvelines, France) (ST6GAL1 217LPP-M0351-Lv242-050-S and negative control 217LPP-NEG-Lv242-025-C). Transductions were carried out according to the manufacturer's instructions using MOI = 5.

### Western blotting

The following antibodies were used: anti-ST6GAL1 (Abgent, AP19891c), anti-β Catenin (Proteintech, Manchester, UK, 51067-2-AP), anti-GAPDH (Abgent, AP7873b), and normal rabbit IgG (711-035-152 Jackson Labs, Bar Harbor, ME, USA). Samples were prepared with 1X Laemmli sample buffer (Bio-Rad, Watford, UK, 161-0747) at a concentration of 10 μg protein in 20 μl. Samples were heated at $95\,°C$ for 5 min, loaded on 10% Mini-PROTEAN® TGX™ precast protein gels (Bio-Rad, 4561034) in standard sodium dodecyl sulfate (SDS) running buffer (Bio-Rad, 1610744) and separated with the Mini-PROTEAN electrophoresis system (Bio-Rad, 1658005EDU). Gels were transferred onto nitrocellulose membranes with the Mini Trans-Blot® Cell (Bio-Rad). Membranes were blocked in 1X Tris buffered saline Tween 20 detergent (TBST) (Bio-Rad, 1610781) with 5% fat-free milk for 1 h, incubated in primary antibody overnight at $4\,°C$ and secondary antibody conjugated to horseradish peroxidase (HRP) for 1 h at room temperature. Washes between incubations were performed in 1X TBST for $5 \times 5$ min. HRP enzyme activity was detected with enhanced chemiluminescent (ECL) substrate (Thermo Fisher, Waltham, MA, USA, 34580).

### RT–qPCR

Cells were harvested and total RNA extracted using TRI Reagent (Invitrogen, Waltham, MA, USA, 15596-026), according to the manufacturer's instructions. RNA was treated with DNase 1 (Ambion, Loughborough, UK, AM2222), and cDNA was generated by reverse transcription of 500 ng total RNA using the Superscript VILO cDNA synthesis kit (Invitrogen, 11754-050). Quantitative PCR (qPCR) was performed in triplicate on cDNA using SYBR® Green PCR Master Mix (Invitrogen, 4309155) using the QuantStudio™ 7 Flex Real-Time PCR System (Life Technologies, Loughborough, UK). Samples were normalised using the average of three reference genes: GAPDH, β-tubulin, and actin. Primer sequences are provided in supplementary material, Table S2.

### Lectin immunofluorescence

Cells were grown onto Lab-Tek™II Chamber Slides (Thermo Scientific, Loughborough, UK, 154453) for

48 h in 10% FBS and 1% P/S-containing medium. Cells were washed with PBS (Gibco, Loughborough, UK, 20012019) before permeabilisation and fixation with ice-cold absolute methanol (Sigma-Aldrich, 67561) for 10 min at $-20\,^{\circ}C$. Next, slides were washed with PBS and blocked with Carbo-Free™ Blocking solution (Vector Laboratories, Newark, CA, USA, SP-5040) for 1 h at room temperature and incubated overnight at $4\,^{\circ}C$ with FITC-conjugated SNA lectin (Vector Labs, FL-1301-2) at 1:200. Finally, slides were washed with PBS and stained with Hoechst (Thermo Scientific, 62249) for 15 min at room temperature. Images were acquired and processed with the ZEISS Axio Imager 3 (Zeiss, Oberkochen, Germany).

## SNA lectin flow cytometry

For all experiments $1 \times 10^6$ cells were incubated with 1 μg/ml fluorescein labelled SNA lectin (Vector Labs, FL-1301-2) in Carbo-Free™ blocking solution (Vector Labs, SP-5040-125) in PBS for 1 h at $4\,^{\circ}C$ in the dark. 1 μg/ml propidium iodide was added to exclude dead cells. Flow cytometry was performed using a BD LSRFortessa flow cytometer using BD FACSDive™ Diva software at the Newcastle University Flow Cytometry Core Facility. For experiments where cells were cultured in conditioned medium, control and ST6GAL1-overexpressing cells were grown to 70% confluence and maintained in serum-free RPMI for 48 h to collect conditioned medium. Wild-type cells at 80% confluency were washed five with PBS and then cultured in conditioned medium in a T25 flask for 24 h.

## Colony formation assays

Cells were trypsinised and plated at a density of 100 cells per 100-mm dish and maintained until colonies of more than 50 cells had formed. Cells were fixed in 10% formalin for 10 min and stained with 0.5% crystal violet for 10 min at room temperature. Colony numbers were manually counted. Three biological repeats were conducted per cell line.

## Invasion assays

Invasion assays were carried out using a Cultrex 96-well basement membrane extract (BME) cell invasion assay (R&D Systems, Abingdon, UK, 3455-096-K). Cells were cultured in serum-free medium for 24 h and then added to the top chamber at 10,000 cells per well. Full culture medium was added to the bottom wells, and plates were incubated at $37\,^{\circ}C$, 5% $CO_2$ for 24 h. Both chambers were washed in 1X wash buffer and incubated with Calcein AM/cell dissociation solution (final concentration: 0.8 μM) at $37\,^{\circ}C$, 5% $CO_2$ for 30 min. The fluorescence of the bottom chamber (invasive cells) was measured against a background control using a Varioskan LUX (Thermo Scientific) microplate reader at excitation 485 nm, emission 520 nm.

## Mouse models

Male NMRI mice (Charles Rivers, Cheshire, UK) were implanted with $1 \times 10^7$ CWR22RV1 cells with ST6GAL1 knockdown by unilateral subcutaneous injection into the flank. Cells were injected in a volume of 100 μl and Matrigel in a 1:1 mixture. Alternatively, male CD-1 nude mice (Charles Rivers) were inoculated at 8 weeks of age with $1 \times 10^7$ PC3 cells with ST6GAL1 overexpression in 50 μl of cell culture medium and Matrigel (Sigma-Aldrich, CLS354234) in a 1:1 mixture. Animals were weighed and tumour volumes monitored by calliper measurement three times a week until the first animal met a humane endpoint. All *in vivo* experiments were reviewed and approved by the relevant institutional animal welfare committees (Newcastle University Animal Welfare and Ethical Review Board) and performed according to the guidelines for welfare set out by an ad hoc committee of the National Cancer Research Institute and national legislation [Animals (Scientific Procedures) Act 1986]. Animals were maintained in individually ventilated cages and handled in lamina flow hoods under specific pathogen-free conditions.

## MS–based proteomics analysis

Cell pellets were lysed with 1.5% SDS lysis buffer containing 1X protease inhibitors (Sigma-Aldrich, PICT) followed by emulsification using a Branson probe sonicator (Thermo Scientific) with an amplitude of 40%, 15 s on followed by 30 s off in cold water. Conditioned medium was concentrated using a speed vacuum (LABCONCO) followed by addition of 25 μl 10% SDS solution. Protein concentration was quantified using BCA protein assay (Thermo Scientific, J63283). Twenty-five micrograms of proteins from the cell lysates and conditioned medium were aliquoted into new 1.5-ml Eppendorf vials. The sample volume was brought up to 50 μl using 50 mM ammonium bicarbonate (Sigma-Aldrich, 11213) followed by vortexing for 15 s. The sample mixture was incubated for 1 h at $65\,^{\circ}C$ containing a final concentration of 10 mM Tris(2-carboxyethyl) phosphine hydrochloride (TCEP) (Sigma-Aldrich, 75259) to reduce cysteine side chains. Then, thiol groups on cysteine side chains were alkylated with a final concentration 15 mM of iodoacetamide (Acros Organics, Waltham, MA, USA, 144-48-9) in the dark for 45 min at room temperature. Proteins were precipitated with 1 ml cold acetone and stored at $-20\,^{\circ}C$ overnight. Precipitated proteins were pelleted via centrifugation at $14,000 \times g$ for 10 min at $4\,^{\circ}C$, reconstituted with 50 μl 50 mM ammonium bicarbonate, and digested using high-grade sequencing trypsin (Thermo Scientific, 90057) in a 1:30 enzyme-to-protein ratio. Samples were incubated at $37\,^{\circ}C$ overnight without shaking.

Tryptic peptides were reconstituted in 50 μl 0.1% formic acid in water. A Dionex Ultimate Rapid Separation liquid chromatography system (Thermo Scientific) was used to inject 3 μl of the tryptic peptides into a 10-μl loop and subsequently loading tryptic

peptides on a C18 PepMap trap column (Thermo Scientific, 164946) at a constant flow rate of 5 μl/min for 10 min. A reversed-phase liquid chromatography gradient consisting of mobile phase A (0.1% formic acid in water) and mobile phase B (0.1% formic acid in acetonitrile) was used to separate tryptic peptides on a 25-cm-long analytical column (New Objective, Littleton, MA, USA) packed in house with Magic C18 AQ resin (Michrom Bioresources Inc, Auburn, CA, USA). The chromatographic programme consisted of holding mobile phase B at 2% for the first 10 min, slowly ramped up to 35% B over 110 min, followed by an increase to 85% B over 2 min with a 7-min hold. The analytical column was re-equilibrated for 20 min prior to the next sample injection. The flow rate was set to 0.5 μl/min throughout the gradient and each sample was analysed in triplicate. Eluted peptides were subjected to electrospray ionisation with an ionisation voltage of 2.0 kV in positive mode using a nanospray Flex ion source (Thermo Scientific) coupled to an Orbitrap Elite (Thermo Scientific). The top 10 most abundant ions per MS1 scan were selected for higher energy collision-induced dissociation (35 eV) in a data-dependent fashion. MS1 resolution was set at 60,000, fourier transform automated gain control (FTAGC) target was set at 1e6, and the $m/z$ scan range was set from $m/z = 400$–1800. MS2 AGC was targeted at 3e4 with a maximum injection time of 200 ms. Dynamic exclusion was enabled for 30 s.

Raw data files were searched by Byonic 2.11.0 (Protein Metrics, San Carlos, CA, USA) against the Swiss-Prot human proteome database [32]. Trypsin digestion with a maximum of two missed cleavages, precursor mass tolerance of 0.5 Da, and fragment mass tolerance of 10 ppm were specified. Additional parameters included fixed cysteine carbamidomethylation, variable methionine oxidation, and asparagine deamination. Only peptide identifications with 1% false discovery rate and identified with two or more spectra were retained for subsequent analysis. Chromatographic runs were aligned, and an R script based on the MSnbase package [33] was used to extract quantitative data from the MS1 spectra of all identified peptides, resulting in the area under the curve (AUC) of the extracted ion current (XIC) of all detected peptides. Changes in protein abundance were then determined using the Generic Integration Algorithm [34], where all quantitative data are expressed as Z-scores at the protein or peptide level. Log2 ratio values were calculated by comparing the AUC of peptides in ST6GAL1 overexpression and control DU145 samples. The weighted, spectrum, peptide, and protein model was used to calculate the corresponding statistical weight at the spectrum level, rescaled, and standardised to a normal distribution $N(0,1)$. Plotting the cumulative distributions was used to carefully examine the validity of the null hypothesis at each level (spectrum, peptide, and protein). Finally, statistical analysis was performed using Student's $t$-test for pairwise comparisons. To identify protein differences from ST6GAL1 overexpression that were concordant in both the secreted medium and cell lysate datasets, we calculated statistical significance based on Pearson correlation.

Proteins with a $p$ value <0.05 were considered significant. The MS proteomics data have been deposited at the ProteomeXchange Consortium via the PRIDE [35] partner repository under the dataset identifier PXD041316.

## Statistical analyses

Statistical analyses were conducted using GraphPad Prism (Dotmatics, Boston, MA, USA, version Prism 9.4.1). Statistical significance is denoted by $*p < 0.05$, $**p < 0.01$, $***p < 0.001$, and $****p < 0.0001$.

# Results

## ST6GAL1 is upregulated in prostate tumour tissue, and larger branched glycans with α2,6 sialylation are common to prostate tumours

We first set out to verify that the ST6GAL1 enzyme was upregulated in prostate tumour tissue. Upregulation of the sialyltransferase ST6GAL1 was previously reported in prostate cancer tissue compared to non-malignant tissue where levels correlated with Gleason grade [36], and we previously published preliminary findings suggesting that *ST6GAL1* levels are upregulated in prostate tumours compared to normal or benign prostate tissue [37,38]. Here, we used immunohistochemistry to measure ST6GAL1 protein levels in matched normal and prostate tumour tissue samples from 200 patients. ST6GAL1 levels were 1.4-fold higher in prostate tumour tissue compared to matched normal tissue from the same patient ($p < 0.001$) (Figure 1A and supplementary material, Figure S1). We confirmed the specificity of our ST6GAL1 antibody via pre-incubation with a blocking peptide and by detection of protein depletion in formalin-fixed paraffin-embedded (FFPE) cell pellets of *ST6GAL1*-shRNA-treated cells (supplementary material, Figure S2). Together with the published literature, these findings confirm upregulation of ST6GAL1 in prostate tumour tissue.

MALDI-IMS can be used to directly and sensitively profile the *N*-glycan composition of FFPE tissues [39], and specific *N*-glycans have been histologically mapped in prostate tumours [26]. The most common tumour-associated *N*-glycans detected by MALDI-IMS are tri- and tetra-antennary structures with or without additional fucose and sialic acids [26]. The above data predicted that the glycan products of ST6GAL1 (α2,6 sialylated *N*-glycans) should also be upregulated in prostate tumours. We tested this using MALDI-IMS to monitor *N*-glycan distributions in pathologist defined FFPE prostate tumour samples and a TMA of prostate tumours [24]. An amidation reaction was performed prior to MALDI-IMS analysis to enable us to differentiate α2,6 from α2,3-linked *N*-linked sialic acids [25]. Initial analysis of prostate tissue samples from two individual patients revealed abundant expression of α2,6 sialylated tri- and tetra-antennary glycans that were specifically localised to areas of prostate tumours (identified by a
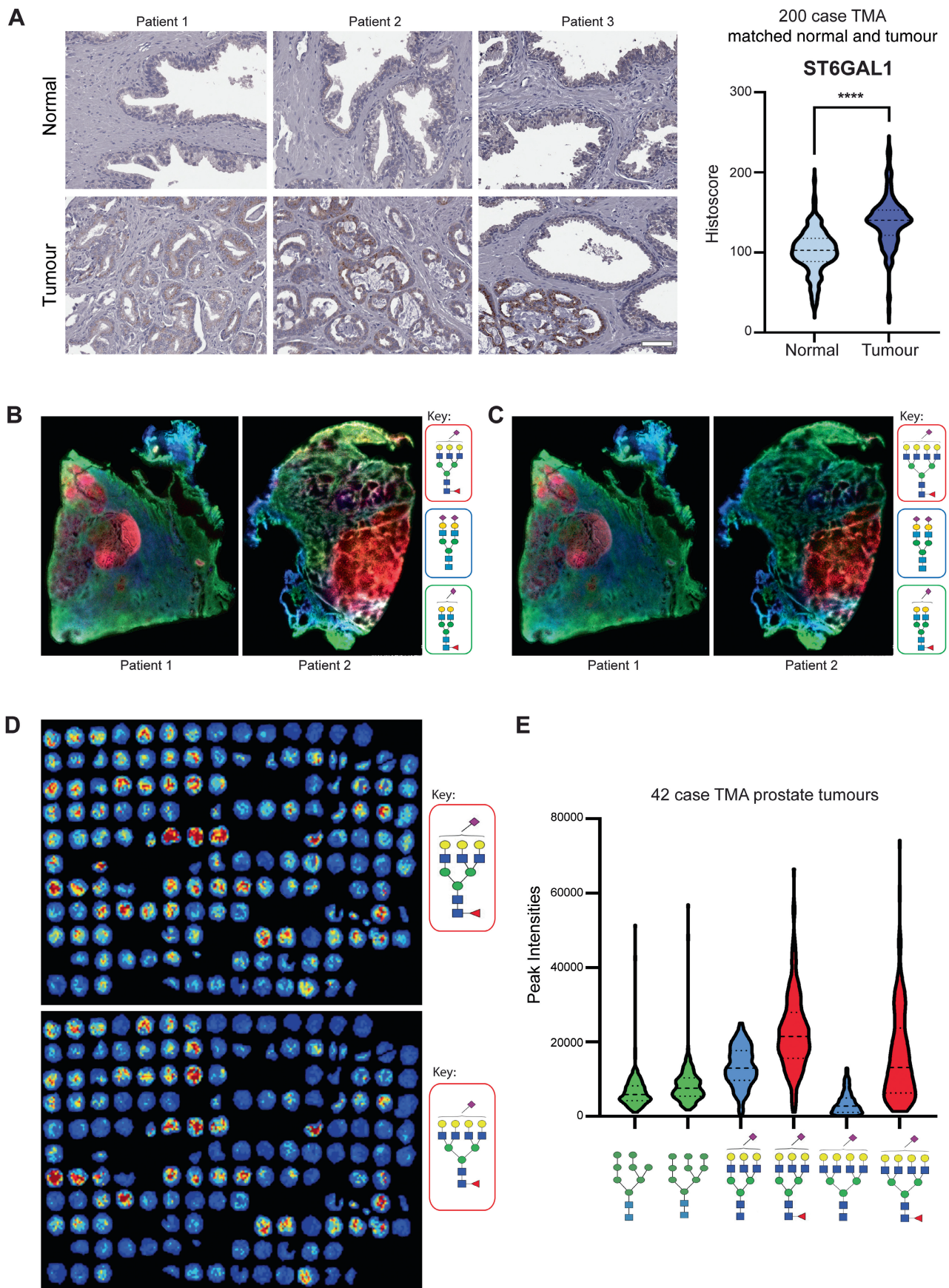
pathologist and shown in red). This contrasts with abundant non-tumour α2,6 sialylated biantennary *N*-glycans (Hex5HexNAc4-α2,6NeuAc localised to the stroma and shown in blue and Hex5HexNAc4Fuc1-α2,6NeuAc shown in green) (Figure 1B,C). Next, comprehensive analysis of *N*-glycan distributions revealed that the same branched α2,6 sialylated tri- and tetra-antennary glycans are commonly found in prostate tumours. The intensity distributions of two α2,6 sialylated tri- and tetra-antennary *N*-glycans are shown in Figure 1D (samples from 42 patients were analysed, with three TMA cores from each patient). The average peak intensities for other *N*-glycans were extracted for each tumour core, and the distributions of select *N*-glycans are shown in Figure 1E. Note the increased detection of branched *N*-glycans in comparison to other common tumour-associated *N*-glycans with high mannose contents [26].

## ST6GAL1 is upregulated in blood samples from men with prostate cancer

The preceding data showed that prostate tumours had upregulation of ST6GAL1 and suggest larger branched *N*-glycans with α2,6 sialylation are common to prostate tumours. In addition to the canonical intracellular ER-Golgi localisation of ST6GAL1, catalytically active enzymes can be released into the extracellular space and systemic circulation from cancer cells [40]. Based on this, and because we recently showed that another glycosyltransferase (GALNT7) was upregulated in the biological fluids of men with prostate cancer [21], we hypothesised that ST6GAL1 might also be secreted into prostate cancer patient blood. To test this, we used pre-validated sandwich ELISA assays (supplementary material, Figure S3) to monitor ST6GAL1 protein levels in 400 plasma samples across three independent cohorts (as each cohort was prepared using differing centrifuge spin speeds and preparation tubes, and this appeared to influence ST6GAL1 levels, it was not possible to compare ST6GAL1 between cohorts). First, we measured ST6GAL1 in plasma samples from 27 men with suspected prostate cancer. ST6GAL1 levels were 48-fold higher in plasma samples taken from men who were later diagnosed with prostate cancer, compared to men with benign disease or a 'no cancer' diagnosis ($p = 0.135$) (Figure 2A). Next, we monitored ST6GAL1 plasma levels in 266 men diagnosed with

either benign prostate hyperplasia (BPH) or prostate cancer. ST6GAL1 protein levels were 2.8-fold higher in men with prostate cancer compared to men diagnosed with BPH ($p = 0.0001$) (Figure 2B). Finally, ST6GAL1 plasma levels were also monitored in 121 men with suspected prostate cancer taking part in the INNOVATE clinical trial [29,30]. Here, plasma ST6GAL1 was 3.5-fold higher in men diagnosed with prostate cancer (compared to men given a 'no cancer' diagnosis) ($p = 0.0413$) (Figure 2C). Taken together, these findings show that ST6GAL1 is upregulated in the blood of men with prostate cancer.

## ST6GAL1 promotes prostate tumour growth and invasion

The data presented above show that ST6GAL1 is upregulated in prostate cancer tissue and that increased levels are detected in the blood of men with prostate cancer. Previous work suggested that ST6GAL1 promoted aggressive prostate cancer cell behaviour *in vitro* [36]. However, the impacts of ST6GAL1 on the biology of prostate cancer cells have not yet been investigated *in vivo*. We created prostate cancer cell lines with stable knockdown or overexpression of ST6GAL1 (supplementary material, Figure S4) and used these to investigate the effects of ST6GAL1. Knockdown of ST6GAL1 in AR positive CWR22RV1 cells inhibited colony formation *in vitro*, whereas overexpression of ST6GAL1 in AR negative PC3 cells had the opposite effect (supplementary material, Figure S5A,B). We obtained similar results using subcutaneous *in vivo* mouse models, where knockdown of ST6GAL1 suppressed the growth of CWR22RV1 tumours (Figure 3A), and overexpression increased the growth of PC3 tumours (Figure 3B). Furthermore, *in vitro* assays showed that ST6GAL1 promoted prostate cancer cell migration and invasion (Figure 3C,D and supplementary material, Figure S5C,D).

Next, we used MS to investigate how increased expression of ST6GAL1 in DU145 cells modified the prostate cancer proteome. This identified 296 differentially expressed proteins (supplementary material, Table S1), including ST6GAL1 itself ($p = 0.04$), and also highlighted 'metabolism', 'immune system', and 'cell signalling' REACTOME pathways as altered in ST6GAL1-overexpressing cells (Figure 3E,F).

**Figure 1.** ST6GAL1 is upregulated in prostate tumour tissue, and larger branched glycans with α2,6 sialylation are common to prostate tumours. (A) Immunohistochemistry of ST6GAL1 in prostate tumour tissue relative to matched normal tissue from the same patient. The graph shows the histoscores from a TMA ($n = 200$, paired *t*-test, $p < 0.001$). Scale bar is 100 μm. (B) Distribution of three *N*-glycans in two Gleason grade 7 (3 + 4) prostate FFPE tissues. Tumour regions are highlighted in red, and this overlaps with the localisation for the tri-antennary glycan Hex6HexNAc5Fuc1-α2,6NeuAc, $m/z = 2,493.917$. Stroma localised, non-tumour α2,6 sialylated biantennary *N*-glycans (Hex5HexNAc4-α2,6NeuAc; $m/z = 1981.728$) are shown in blue and Hex5HexNAc4Fuc1-α2,6NeuAc; $m/z = 2,127.754$ in green. (C) Distribution in red for tetra-antennary tumour glycan Hex7HexNAc6Fuc1-α2,6NeuAc, $m/z = 2,859.054$, and the same biantennary glycans in blue and green. The tumour region (identified by a pathologist) is highlighted in red. (D) *N*-glycan IMS intensity distributions of the tri- and tetra-antennary glycans ($m/z = 2,493.917$ and $2,859.054$) in TMA slide ($n = 42$ patients, three cores per patient). (E) Intensities of six tumour *N*-glycans from 136 individual tumour cores. Structures of each glycan are shown on the *x*-axis for $m/z = 1743.560$, high-mannose Man8; $m/z = 1905.618$, high-mannose Man9; $m/z = 2,346.799$ Hex6HexNAc5-α2,6NeuAc; $m/z = 2,493.917$, Hex6HexNAc5Fuc1-α2,6NeuAc, $m/z = 2,711.988$, Hex7HexNAc6-α2,6NeuAc; $2,859.018$, Hex7HexNAc6Fuc1-α2,6NeuAc.
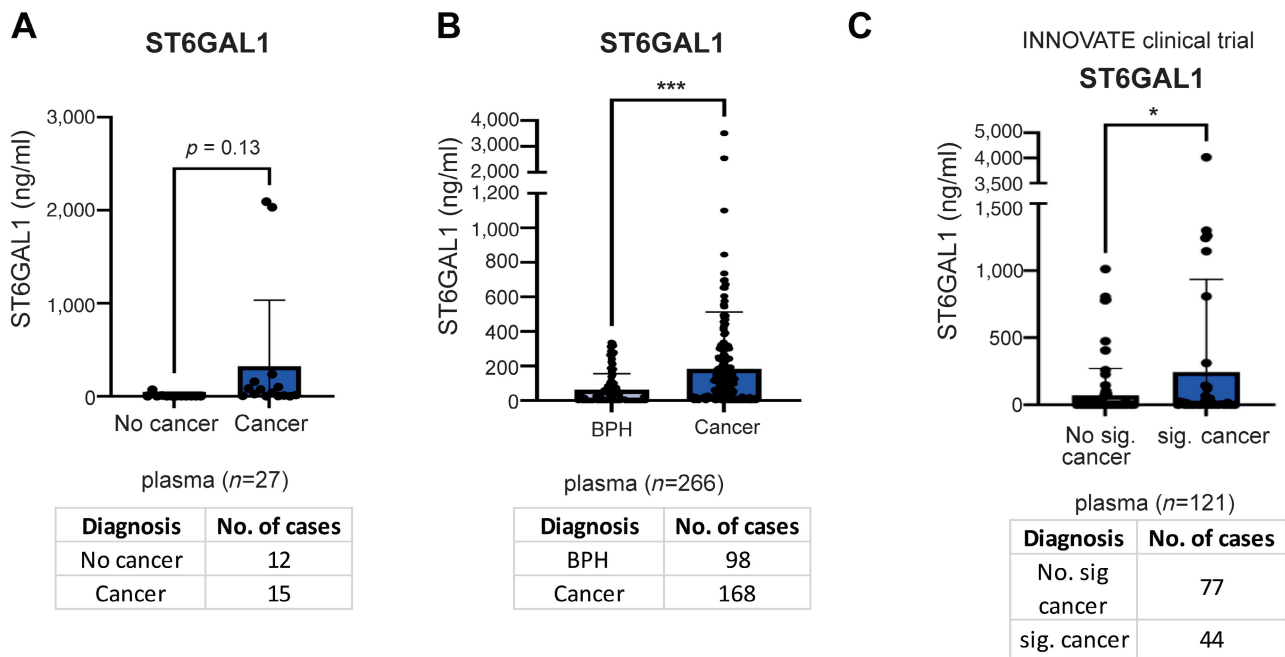
**A**     ST6GAL1

**B**     ST6GAL1

**C**     INNOVATE clinical trial ST6GAL1

| Diagnosis | No. of cases |
|-----------|--------------|
| No cancer | 12 |
| Cancer | 15 |

| Diagnosis | No. of cases |
|-----------|--------------|
| BPH | 98 |
| Cancer | 168 |

| Diagnosis | No. of cases |
|-----------|--------------|
| No. sig cancer | 77 |
| sig. cancer | 44 |

Figure 2. ST6GAL1 is upregulated in the blood of men with prostate cancer. (A–C) Detection of ST6GAL1 in plasma samples using sandwich ELISA (data shown as mean ± SD). Samples from men (A) with suspected prostate cancer ($p = 0.135$ unpaired $t$-test, $n = 27$), (B) with prostate cancer compared to BPH ($p = 0.004$, unpaired $t$-test, $n = 266$), (C) who were diagnosed with clinically significant prostate cancer (sig. cancer) compared to men who received a 'no significant cancer' (no sig. cancer) diagnosis cancer in INNOVATE clinical trial (30, 31) ($p = 0.0413$ unpaired $t$-test, $n = 121$).

Consistent with previous findings [36], we detected a correlation between ST6GAL1 and β-catenin signalling (Figure 3G). Of particular interest, levels of the cell adhesion glycoprotein CD44 increased in response to ST6GAL1 overexpression (Figure 3H), and there was a correlation between *ST6GAL1* and *CD44* mRNA levels in clinical prostate cancer tissue [41,42] (Figure 3I).

## ST6GAL1 regulates α2,6-linked sialylation of *N*-glycans in prostate cancer cells

ST6GAL1 adds α2,6-linked sialic acid to *N*-glycosylated proteins destined for the plasma membrane or secretion [18,19]. To test whether upregulation of ST6GAL1 altered α2,6 sialylation of *N*-glycans in prostate cancer cells, we assessed glycan recognition by SNA, the lectin from *Sambucus nigra* (which recognises α2,6-linked sialylated *N*-glycans [43]) using our ST6GAL1 prostate cancer cell line models. SNA cell staining and flow cytometry revealed that ST6GAL1 knockdown reduced binding, whereas ST6GAL1 overexpression correlates with increased binding of SNA lectin (Figure 4A,B), indicating that upregulation of ST6GAL1 introduces α2,6 sialylated *N*-glycans on prostate cancer cells. Recent findings showed ST6GAL1 was released into the extracellular milieu and could act extracellularly to modify cell surface and secreted glycans [40]. Based on this, we hypothesised that prostate cancer cells could secrete ST6GAL1 and this enzyme could act extrinsically to remodel cell surface glycans on other cells. To test this, we treated wild-type prostate cancer cells with (1) recombinant ST6GAL1 enzyme

and (2) conditioned medium from prostate cancer cells overexpressing ST6GAL1 and monitored the effects of extracellular ST6GAL1 on the prostate cancer glycome. These experiments showed that both extracellular ST6GAL1 enzyme and conditioned medium from prostate cancer cells with upregulated ST6GAL1 enhanced α2,6 sialylation of *N*-glycans of wildtype prostate cancer cells, indicating that prostate cancer cells can secrete active ST6GAL1 enzyme capable of remodelling glycans on the surface of other cells (Figure 4C–F). Taken together, the data show that ST6GAL1 regulates α2,6-linked sialylation of *N*-glycans in prostate cancer cells and suggest the existence of an extracellular function for ST6GAL1 in prostate cancer.

## The sialyltransferase inhibitor 3F$_{ax}$-Neu5Ac blocks α2,6-linked sialylation of *N*-glycans in prostate cancer cells

The findings presented above identify higher levels of ST6GAL1 and specific α2,6-linked sialylated *N*-glycans in prostate tumours compared to normal prostate tissue, suggesting these could be potential therapeutic targets for prostate cancer. To address this, we assessed the effect of P-3F$_{AX}$-Neu5Ac, a cell-permeable global metabolic inhibitor of sialylation [44,45]. Both immunocytochemistry and lectin flow cytometry showed that 3F$_{ax}$-Neu5Ac treatment significantly reduced the binding of SNA lectin to both CWR22RV1 and PC3 cells (Figure 5A,B). Furthermore, *in vitro* assays showed sialic acid blockade inhibited prostate cancer cell colony formation (Figure 5C,D). Taken together,
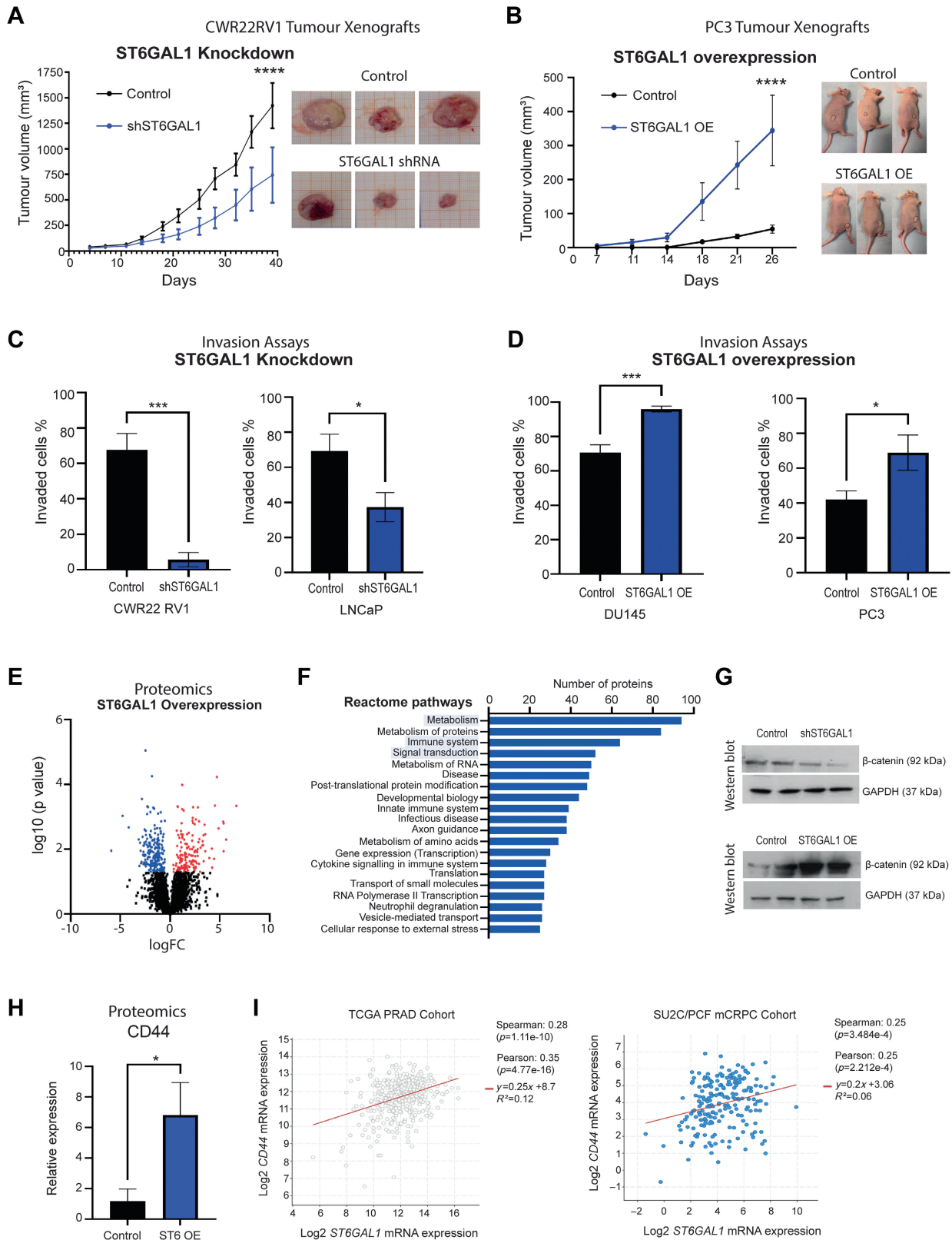
**Figure 3.** ST6GAL1 promotes prostate tumour growth and cell invasion. (A) Growth of CWR22RV1 tumour xenografts with or without knockdown of ST6GAL1 using shRNA ($p < 0.001$, two-way ANOVA, $n = 6$ mice per group). Representative images are shown for each group. (B) Growth of PC3 cell xenograft tumours with or without upregulation of ST6GAL1 ($p < 0.001$, two-way ANOVA, $n = 8$ mice per group). Representative images are shown for each group and the outline of each tumour is marked. (C and D) Impacts of knockdown and overexpression of ST6GAL1 on prostate cancer cell invasion. Six technical and two biological repeats were carried out for each experiment, and representative results are shown. (E) MS proteomics analysis of DU145 cells with upregulation of ST6GAL1. (F) Reactome pathway analysis of these 296 proteins. (G) Western blotting of β-catenin in cells with ST6GAL1 knockdown or overexpression. (H) The effect of ST6GAL1 upregulation on CD44 levels ($p < 0.001$). (I) Correlation between *ST6GAL1* and *CD44* mRNA levels in The Cancer Genome Atlas PRAD cohort (32) and CRPC Stand Up to Cancer/Prostate Cancer Foundation (SU2C/PCF) cohort (33).
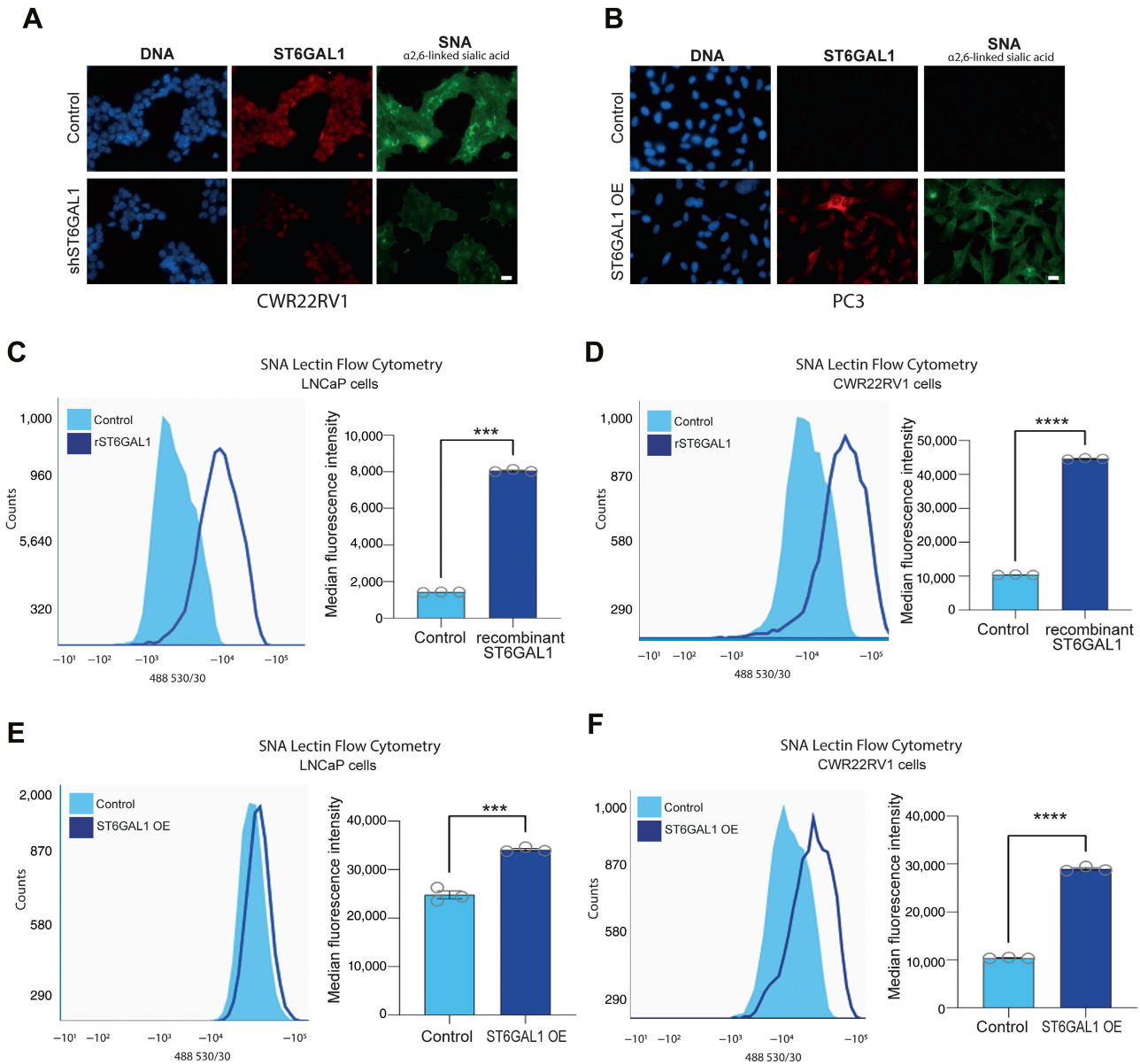
**Figure 4.** ST6GAL1 regulates α2,6-linked sialylated *N*-glycans in prostate cancer cells. (A and B) Detection of α2,6-linked sialylated *N*-glycans using SNA lectin in (A) CWR22Rv1 cells with knockdown of ST6GAL1 and (B) PC3 cells with overexpressed ST6GAL1. (C and D) SNA lectin flow cytometry of control cells or cells treated with 2 μg/ml recombinant ST6GAL1 (C) LNCaP cellds. (D) CWR22RV1 cells. (E and F) SNA lectin flow cytometry of cells treated with conditioned medium from control or ST6GAL1-overexpressing cells; (E) LNCaP cells, (F) CWR22RV1 cells. For panels C–F, three technical and three biological repeats were performed for each experiment and representative data are shown.

these data show that the sialyltransferase inhibitor P-3F$_{AX}$-Neu5Ac can inhibit α2,6-linked sialylation of *N*-glycans in prostate cancer cells and highlight the potential to inhibit aberrant sialylation to develop new treatments for prostate cancer.

## Discussion

Tumour cells often have increased levels of sialylation, which leads to a dense forest of sialylated structures covering the cell surface [18]. This hypersialylation has far-reaching consequences for cancer cells, but the role of abnormal sialylation in disease progression remains

poorly understood in prostate cancer. An increased understanding of how sialylated glycans impact prostate cancer biology will open new opportunities for disease intervention and facilitate the development of new therapeutics. In this study, we verified the upregulation of the sialyltransferase enzyme ST6GAL1 and identified specific branched α2,6 sialylated *N*-glycans that are common in prostate tumour tissues. Furthermore, we revealed increased levels of ST6GAL1 in the blood of men with prostate cancer. ST6GAL1 adds sialic acids in an α2,6 linkage to galactose residues on *N*-glycans and is the most well-described sialyltransferase in humans [17]. A previous study demonstrated ST6GAL1 was upregulated in aggressive prostate cancer tissue and was associated with reduced patient survival [36]. Our
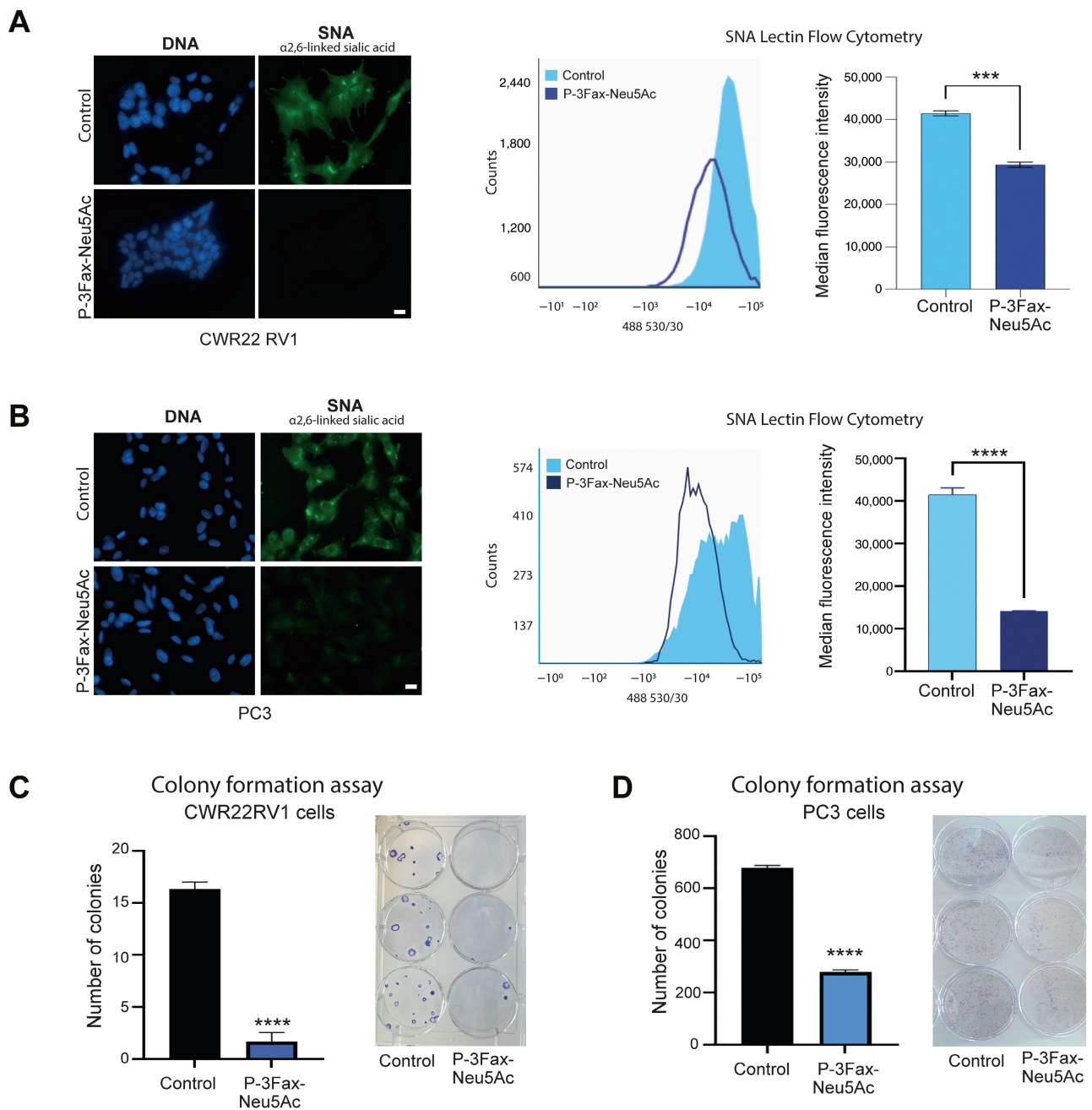
**Figure 5.** Inhibition of α2,6-linked sialylation of *N*-glycans in prostate cancer cells using the sialyltransferase inhibitor P-3F$_{AX}$–Neu5Ac. (A and B) Detection of α2,6-linked sialylated *N*-glycans using SNA lectin in CWR22RV1 and PC3 cells with 200 μM P-3FaX-Neu5Ac. (C and D) Colony formation after sialic acid blockade using P-3FaX-Neu5Ac. For all experiments, three technical and three biological repeats were performed and representative data are shown.

data confirmed the upregulation of ST6GAL1 in prostate tumour tissue, identified larger branched glycans with α2,6 sialylation as common, and revealed a previously undescribed phenomenon; the levels of extracellular ST6GAL1 are also significantly increased in prostate cancer patients. This finding is consistent with previous results suggesting glycosyltransferases could be shed by tumour cells [40,46–48] and that certain cancer cells have the ability to raise the levels of extracellular ST6GAL1 [40,49].

Our study identified ST6GAL1 as a key driver of prostate cancer invasion and tumour growth. These findings are in agreement with, and build upon, a previous *in vitro* study where ST6GAL1 was reported to regulate aggressive prostate cancer cell behaviour and, to our knowledge, is the first time the impact of ST6GAL1 on prostate cancer biology has been studied *in vivo*. Of particular interest, knockdown of ST6GAL1 in CWR22RV1 prostate cancer cells suppressed the growth of subcutaneous implants, thereby identifying ST6GAL1 and its associated glycans as potential therapeutic targets for prostate cancer. Previous studies suggested that ST6GAL1 could alter cellular function via sialylation of various surface receptors, resulting in

altered signal transduction [50]. Our findings show that ST6GAL1 activity modifies the proteome of prostate cancer cells and correlates with the expression of key regulators of cell signalling, including β-catenin and CD44 [36,40]. β-catenin is a pivotal component of the Wnt signalling pathway linked to early events in carcinogenesis [51], and CD44 is a cell adhesion glycoprotein that governs cell signalling and is often dysregulated in cancer [52,53]. These data suggest that ST6GAL1-mediated sialylation may orchestrate oncogenic signalling pathways in prostate cells and point to the need for greater delineation of specific signalling mechanisms.

Canonically, ST6GAL1 is localised within the Golgi network, and it is within this context that the role of ST6GAL1 in tumour biology has been examined. However, catalytically active ST6GAL1 is also present extracellularly [40]. Initial studies suggested that circulating ST6GAL1 was released by the liver [54], but recent findings show breast cancer cells can release functional ST6GAL1 [40]. ST6GAL1 is present in exosomes and other extracellular vesicles (EVs) [55], and when tumour cells take up EV-derived ST6GAL1, they acquire elevated sialylation and undergo phenotypic remodelling. Based on this, along with the findings presented in this manuscript, we propose that prostate cancer cells may also release ST6GAL1, and this extracellular enzyme may modify the sialylation and cell signalling pathways in recipient target cells. This suggests a complex mechanism of ST6GAL1-mediated prostate cancer progression and also raises the possibility of targeting extracellular ST6GAL1 therapeutically.

The development of strategies to inhibit aberrant sialylation in cancer represents an important opportunity to develop new therapeutics. Consistent with this, we showed that ST6GAL1 regulated α2,6-linked sialylated *N*-glycans in prostate cancer cells leading to an increased level of sialylation on the cell surface. Furthermore, we showed that sialylation of prostate cells could be inhibited using the global sialyltransferase inhibitor P-3F$_{AX}$-Neu5Ac. Previous studies showed that intra-tumoural injection of P-3F$_{AX}$-Neu5Ac could suppress tumour growth in multiple tumour types [56], and targeted delivery of P-3F$_{AX}$-Neu5Ac using nanoparticles prevented metastasis in a mouse lung cancer model [57]. In addition, further derivatives of P-3F$_{AX}$-Neu5Ac have now been developed, including carbamate sialyltransferase inhibitors that reach higher concentrations within cells and induce prolonged inhibition of sialylation [58]. Together, these studies highlight the potential to explore the use of sialylation inhibitors as new therapeutics for prostate cancer.

In addition to sialylation inhibitors, other strategies to target aberrant sialylation in cancer are also being explored. These include antibody–sialidase conjugates, Selectin inhibitors, and anti-Siglec antibodies and vaccines [59]. Antibody–sialidase conjugates have been used to remove sialylated glycans on breast cancer cells to enhance immune cell activation and improve survival times in mice with trastuzumab-resistant breast cancer [59–62], and this is being further evaluated in clinical trials in combination with traditional immune checkpoint blockade (NCT05259696). Strategies to inhibit altered sialylation that are being developed for other cancers are also likely applicable to prostate cancer, and it is interesting to speculate that approaches such as those described above could be used to selectively de-sialylate prostate cancer cells and induce an anti-tumour response.

Here, we established a role for ST6GAL1-mediated aberrant sialylation in prostate cancer progression. Moving forward, and given the explosion of data implicating sialylated glycans in immune evasion [59], it will be essential to study the role of ST6GAL1 in the prostate in the context of a functional immune system. In addition, as numerous studies in other cancer types have linked ST6GAL1 to aggressive disease and metastasis, preclinical models to investigate the importance of ST6GAL1 in prostate cancer metastasis will likely also provide clinically actionable information. Increased sialylation is a common feature of tumours and can also contribute to chemotherapy and radiotherapy resistance in a range of tumour backgrounds. The groundwork has been laid for the development of new strategies to target sialylated glycans in cancer, and there exists potential to explore these in combination with existing therapies for prostate cancer.

In conclusion, prostate cancer is the most common cancer in men and a major clinical burden. There remains an unmet clinical need to develop new therapeutic strategies for advanced disease, and targeting aberrant sialylation represents an important and as yet unexplored clinical opportunity. The sialome acts as an essential interface between prostate cancer cells and the surrounding microenvironment and likely plays an important functional role in tumour pathology. Our study cements ST6GAL1 and α2,6 sialylation as important drivers of prostate cancer progression and points to the development of new therapeutics targeting ST6GAL1 and/or its associated glycans. Numerous therapeutic strategies are under development to target aberrant sialylation in cancer, and new studies exploring the role of ST6GAL1 in prostate cancer biology will be vital to ensure men with prostate cancer can benefit from these advances.

## Acknowledgements

## Author contributions statement

ES, EAG, RG, KH, MOM, KPN, KL, AB, FJGM, AD, AH, AD, KB and GH performed *in vitro* experiments. ES, HT, HMA and NW performed the *in vivo* studies. HP, SH, USF, AH, AF, SS, EWJ, SP, BK, PM, JM, MC, LH, FF, NM, DAT and HW contributed to clinical sample collection. ULM and LW performed IHC on tissue sections. HT and ULM scored pathology sections. RRD performed N-glycan MALDI-IMS. JM and ES designed, analysed, and interpreted the study. JM wrote the manuscript and created the figures. RRD, DJE, ES, RH, SP and NW contributed to critical review and paper writing. JM conceived the study and is senior author and corresponding author. All authors read the manuscript, agreed with the content, and were given the opportunity to provide input.

## Data availability statement

The authors confirm that the data supporting the findings of this study are available within the article and its supplementary materials.

## References

1. Siegel RL, Miller KD, Jemal A. Cancer statistics, 2016. *CA Cancer J Clin* 2016; **66:** 7–30.

2. Livermore K, Munkley J, Elliott DJ. Androgen receptor and prostate cancer. *AIMS Molecular Science* 2016; **3:** 280–299.

3. de Bono JS, Logothetis CJ, Molina A, *et al*. Abiraterone and increased survival in metastatic prostate cancer. *N Engl J Med* 2011; **364:** 1995–2005.

4. Ryan CJ, Molina A, Griffin T. Abiraterone in metastatic prostate cancer. *N Engl J Med* 2013; **368:** 1458–1459.

5. Beer TM, Tombal B. Enzalutamide in metastatic prostate cancer before chemotherapy. *N Engl J Med* 2014; **371:** 1755–1756.

6. Scher HI, Fizazi K, Saad F, *et al*. Increased survival with enzalutamide in prostate cancer after chemotherapy. *N Engl J Med* 2012; **367:** 1187–1197.

7. Fizazi K, Shore N, Tammela TL, *et al*. Darolutamide in nonmetastatic, castration-resistant prostate cancer. *N Engl J Med* 2019; **380:** 1235–1246.

8. Morote J, Aguilar A, Planas J, *et al*. Definition of castrate resistant prostate cancer: new insights. *Biomedicine* 2022; **10:** 689.

9. Varki A, Kornfeld S. Historical background and overview. In *Essentials of Glycobiology* (4th edn), Varki A, Cummings RD, Esko JD, *et al*. (eds). Cold Spring Harbor: New York, 2022; 1–20.

10. Möckl L. The emerging role of the mammalian glycocalyx in functional membrane organization and immune system regulation. *Front Cell Dev Biol* 2020; **8:** 253.

11. Pinho SS, Reis CA. Glycosylation in cancer: mechanisms and clinical implications. *Nat Rev Cancer* 2015; **15:** 540–555.

12. Gagneux P, Hennet T, Varki A. Biological functions of Glycans. In *Essentials of Glycobiology*, Varki A, Cummings RD, *et al*. (eds). Cold Spring Harbor: New York, 2022; 79–92.

13. Munkley J, Elliott DJ. Hallmarks of glycosylation in cancer. *Oncotarget* 2016; **7:** 35478–35489.

14. Mereiter S, Balmaña M, Campos D, *et al*. Glycosylation in the era of cancer-targeted therapy: where are we heading? *Cancer Cell* 2019; **36:** 6–16.

15. Rodrigues E, Macauley MS. Hypersialylation in cancer: modulation of inflammation and therapeutic opportunities. *Cancers (Basel)* 2018; **10:** 207.

16. Pearce OM, Laubli H. Sialic acids in cancer biology and immunity. *Glycobiology* 2016; **26:** 111–128.

17. Dorsett KA, Marciel MP, Hwang J, *et al*. Regulation of ST6GAL1 sialyltransferase expression in cancer cells. *Glycobiology* 2021; **31:** 530–539.

18. Munkley J. Aberrant sialylation in cancer: therapeutic opportunities. *Cancers (Basel)* 2022; **14:** 4248.

19. Garnham R, Scott E, Livermore KE, *et al*. ST6GAL1: a key player in cancer. *Oncol Lett* 2019; **18:** 983–989.

20. Munkley J, Scott E. Targeting aberrant sialylation to treat cancer. *Medicines (Basel)* 2019; **6:** 102.

21. Scott E, Hodgson K, Calle B, *et al*. Upregulation of GALNT7 in prostate cancer modifies O-glycosylation and promotes tumour growth. *Oncogene* 2023; **42:** 926–937.

22. Kirkegaard T, Edwards J, Tovey S, *et al*. Observer variation in immunohistochemical analysis of protein expression, time for a change? *Histopathology* 2006; **48:** 787–794.

23. Munkley J, McClurg UL, Livermore KE, *et al*. The cancer-associated cell migration protein TSPAN1 is under control of androgens and its upregulation increases prostate cancer cell migration. *Sci Rep* 2017; **7:** 5249.

24. Hawley S, Fazli L, McKenney JK, *et al*. A model for the design and construction of a resource for the validation of prognostic prostate cancer biomarkers: the canary prostate cancer tissue microarray. *Adv Anat Pathol* 2013; **20:** 39–44.

25. Holst S, Heijs B, de Haan N, *et al*. Linkage-specific in situ sialic acid derivatization for N-glycan mass spectrometry imaging of formalin-fixed paraffin-embedded tissues. *Anal Chem* 2016; **88:** 5904–5913.

26. Blaschke CRK, Hartig JP, Grimsley G, *et al*. Direct N-glycosylation profiling of urine and prostatic fluid glycoproteins and extracellular vesicles. *Front Chem* 2021; **9:** 734280.

27. Drake RR, Powers TW, Norris-Caneda K, *et al*. In situ imaging of N-glycans by MALDI imaging mass spectrometry of fresh or formalin-fixed paraffin-embedded tissue. *Curr Protoc Protein Sci* 2018; **94:** e68.

28. McDowell CT, Klamer Z, Hall J, *et al*. Imaging mass spectrometry and lectin analysis of N-linked glycans in carbohydrate antigen-defined pancreatic cancer tissues. *Mol Cell Proteomics* 2021; **20:** 100012.

29. Johnston E, Pye H, Bonet-Carne E, *et al*. INNOVATE: a prospective cohort study combining serum and urinary biomarkers with novel diffusion-weighted magnetic resonance imaging for the prediction and characterization of prostate cancer. *BMC Cancer* 2016; **16:** 816.

30. Pye H, Singh S, Norris JM, *et al*. Evaluation of PSA and PSA density in a multiparametric magnetic resonance imaging-directed diagnostic pathway for suspected prostate cancer: the INNOVATE trial. *Cancers (Basel)* 2021; **13:** 1985.

31. Munkley J, Li L, Krishnan SRG, *et al*. Androgen-regulated transcription of ESRP2 drives alternative splicing patterns in prostate cancer. *Elife* 2019; **8:** e47678.

32. Breuza L, Poux S, Estreicher A, *et al*. The UniProtKB guide to the human proteome. *Database* 2016; **2016:** bav120.

33. Gatto L, Lilley KS. MSnbase-an R/Bioconductor package for isobaric tagged mass spectrometry data visualization, processing and quantitation. *Bioinformatics* 2012; **28:** 288–289.

34. Navarro P, Trevisan-Herraz M, Bonzon-Kulichenko E, *et al*. General statistical framework for quantitative proteomics by stable isotope labeling. *J Proteome Res* 2014; **13:** 1234–1247.

35. Perez-Riverol Y, Bai J, Bandla C, *et al*. The PRIDE database resources in 2022: a hub for mass spectrometry-based proteomics evidences. *Nucleic Acids Res* 2022; **50:** D543–D552.

36. Wei A, Fan B, Zhao Y, *et al*. ST6Gal-I overexpression facilitates prostate cancer progression via the PI3K/Akt/GSK-3β/β-catenin signaling pathway. *Oncotarget* 2016; **7:** 65374–65388.

37. Munkley J. Glycosylation is a global target for androgen control in prostate cancer cells. *Endocr Relat Cancer* 2017; **24:** R49–R64.

38. Munkley J, Vodak D, Livermore KE, *et al*. Glycosylation is an androgen-regulated process essential for prostate cancer cell viability. *EBioMedicine* 2016; **8:** 103–116.

39. McDowell CT, Lu X, Mehta AS, *et al*. Applications and continued evolution of glycan imaging mass spectrometry. *Mass Spectrom Rev* 2021; **42:** 674–705.

40. Hait NC, Maiti A, Wu R, *et al*. Extracellular sialyltransferase st6gal1 in breast tumor cell growth and invasiveness. *Cancer Gene Ther* 2022; **29:** 1662–1675.

41. Hoadley KA, Yau C, Hinoue T, *et al*. Cell-of-origin patterns dominate the molecular classification of 10,000 tumors from 33 types of cancer. *Cell* 2018; **173:** 291–304 e296.

42. Abida W, Cyrta J, Heller G, *et al*. Genomic correlates of clinical outcome in advanced prostate cancer. *Proc Natl Acad Sci U S A* 2019; **116:** 11428–11436.

43. Bojar D, Meche L, Meng G, *et al*. A useful guide to lectin binding: machine-learning directed annotation of 57 unique lectin specificities. *ACS Chem Biol* 2022; **17:** 2993–3012.

44. Rillahan CD, Antonopoulos A, Lefort CT, *et al*. Global metabolic inhibitors of sialyl- and fucosyltransferases remodel the glycome. *Nat Chem Biol* 2012; **8:** 661–668.

45. Büll C, Boltje TJ, Wassink M, *et al*. Targeting aberrant sialylation in cancer cells using a fluorinated sialic acid analog impairs adhesion, migration, and in vivo tumor growth. *Mol Cancer Ther* 2013; **12:** 1935–1946.

46. Sun X, Mahajan D, Chen B, *et al*. A quantitative study of the Golgi retention of glycosyltransferases. *J Cell Sci* 2021; **134:** jcs258564.

47. Lichtenthaler SF, Lemberg MK, Fluhrer R. Proteolytic ectodomain shedding of membrane proteins in mammals-hardware, concepts, and recent developments. *EMBO J* 2018; **37:** e99456.

48. Hirata T, Takata M, Tokoro Y, *et al*. Shedding of N-acetylglucosaminyltransferase-V is regulated by maturity of cellular N-glycan. *Commun Biol* 2022; **5:** 743.

49. Myojin Y, Kodama T, Maesaka K, *et al*. ST6GAL1 is a novel serum biomarker for lenvatinib-susceptible FGF19-driven hepatocellular carcinoma. *Clin Cancer Res* 2021; **27:** 1150–1161.

50. Gc S, Bellis SL, Hjelmeland AB. ST6Gal1: oncogenic signaling pathways and targets. *Front Mol Biosci* 2022; **9:** 962908.

51. Zhang Y, Wang X. Targeting the Wnt/β-catenin signaling pathway in cancer. *J Hematol Oncol* 2020; **13:** 165.

52. Chen C, Zhao S, Karnad A, *et al*. The biology and role of CD44 in cancer progression: therapeutic implications. *J Hematol Oncol* 2018; **11:** 64.

53. Iczkowski KA. Cell adhesion molecule CD44: its functional roles in prostate cancer. *Am J Transl Res* 2010; **3:** 1–7.

54. Jones MB, Oswald DM, Joshi S, *et al*. B-cell-independent sialylation of IgG. *Proc Natl Acad Sci U S A* 2016; **113:** 7207–7212.

55. Zhang Q, Higginbotham JN, Jeppesen DK, *et al*. Transfer of functional cargo in exomeres. *Cell Rep* 2019; **27:** e946.

56. Büll C, Boltje TJ, Balneger N, *et al*. Sialic acid blockade suppresses tumor growth by enhancing T-cell-mediated tumor immunity. *Cancer Res* 2018; **78:** 3574–3588.

57. Büll C, Boltje TJ, van Dinther EA, *et al*. Targeted delivery of a sialic acid-blocking glycomimetic to cancer cells inhibits metastatic spread. *ACS Nano* 2015; **9:** 733–745.

58. Heise T, Pijnenborg JFA, Büll C, *et al*. Potent metabolic sialylation inhibitors based on C-5-modified fluorinated sialic acids. *J Med Chem* 2019; **62:** 1014–1021.

59. Smith BAH, Bertozzi CR. The clinical impact of glycobiology: targeting selectins, siglecs and mammalian glycans. *Nat Rev Drug Discov* 2021; **20:** 217–243.

60. Xiao H, Woods EC, Vukojicic P, *et al*. Precision glycocalyx editing as a strategy for cancer immunotherapy. *Proc Natl Acad Sci U S A* 2016; **113:** 10304–10309.

61. Daly J, Carlsten M, O'Dwyer M. Sugar free: novel immunotherapeutic approaches targeting siglecs and sialic acids to enhance natural killer cell cytotoxicity against cancer. *Front Immunol* 2019; **10:** 1047.

62. Gray MA, Stanczak MA, Mantuano NR, *et al*. Targeted glycan degradation potentiates the anticancer immune response in vivo. *Nat Chem Biol* 2020; **16:** 1376–1384.

## SUPPLEMENTARY MATERIAL ONLINE

**Figure S1.** Clinical information for the 200-case tissue microarray shown in Figure 1A

**Figure S2.** Validation of ST6GAL1 antibody for immunohistochemistry

**Figure S3.** Validation of ST6GAL1 sandwich ELISA

**Figure S4.** Validation of ST6GAL1 stable cell lines

**Figure S5.** ST6GAL1 promotes colony formation and migration in prostate cancer cells

**Table S1.** Mass spectrometry proteomics of DU145 prostate cancer cells with upregulation of ST6GAL1

**Table S2.** Real-time PCR primer sequences